JOURNAL OF MODERN OPTICS, 1992, VOL. 39, NO. 8, 1749–1760

Focal images formed by a concave holographic grating. A corroborative investigation using three different techniques

L. TSONEV and E. POPOV

Institute for Solid State Physics, Bulgarian Academy of Sciences, blvd. Trakia 72, 1784 Sofia, Bulgaria

(*Received 22 December 1991; revision received 7 April 1992*)

Abstract. Photographic registration, ray tracing and analytical modelling are used simultaneously for a systematic investigation of focal images generated by a spherical diffraction grating under point source illumination. Special attention is devoted to the case when a circular entrance pupil is located out of the meridional plane. Good correspondence between the three techniques is observed and the meaning of some specific aberration coefficients is clarified. The reliability of two recently proposed formulae for focal spot dimensional estimation is verified over a wide spectral interval.

1. Introduction

The concave grating was originally proposed by Rowland [1–3] in order to combine two functions—dispersion and imaging. After receiving a polychromatic divergent illumination from the device input (circular pupil or narrow slit) the grating generates a set of separated monochromatic images at the device output (fibre, slit, flat field detector).

The image of a slit can be regarded as a set of images of several point sources located on a vertical line at the device input [4, 5], therefore the investigation of the image of an elementary point source and its aberration deformations has a fundamental importance for the understanding of concave gratings as well as for their applications.

The basic requirement for a spectroscopic device is the good spatial resolution in the dispersion (meridional, tangential, horizontal) plane: when the period is fixed, the narrower the focal image spots are, the better is the resolution. Another important requirement is the minimization of energy loss from astigmatic image extension. Thus the knowledge of focal spot dimensions (and form) is vital both for the designer and for the use of the concave grating.

The most widely used method for the evaluation of focal image form and dimensions is indirect and consists in their numerical modelling by ray tracing procedures. The image of the slit is modelled sometimes as an entire object [6–8], but very often as a vertical (sagittal) combination of a few separate images of a point source, placed successively in and out of the meridional plane [4, 9–12]. Such analysis is often complemented by cross-sectional ray densitograms characterizing only the line image width [4, 7, 9, 10, 13–15] and representing one-dimensional approach to grating examination. Some researchers, however, restrict their ray tracing investigation only to images of a point source in the meridional plane and do not discuss the slit image at all [16–19].

0950-0340/92 $3·00

Occasionally, numerical predictions for concave gratings are accompanied by direct observations of experimentally obtained focal images. Two techniques are applied—photographic and photoelectric.

The photographic registration is a classic spectroscopic procedure yielding a full and practically analogous (see, for example, [21] for resolution data) two-dimensional picture of the spectral line, i.e. an image of the entrance slit as a whole. Slit width values between 5 and 50 μm are most often mentioned in the literature about focusing gratings [8, 13, 21–23]. In some specific cases the testing of stigmatic properties requires the illuminating beam to come from a pinhole lying in the meridional (dispersion) plane; the pinhole diameter is reported to be between 60 and 300 μm [13, 20, 24–26]. We have found only one reference to the photographed image of a circular meridional pinhole (with diameter 100 μm) compared with the spot shape predicted by ray tracing—in [20], where a rectangular grating for a Seya–Namioka monochromator was studied. Due to the non-ideal imaging (i.e. to the presence of uncorrected aberrations) the specific shape of the pinhole image is considerably influenced by the form of the diffractive area.

The second experimental technique—the electronic one—is used in two versions. The first version is the traditional continuous spectra scanning by a photomultiplier, which gives analogous one-dimensional cross-sectional information about the focal images [4, 20, 25, 27, 28]. Such experiments are performed with slit width values in the interval 10–100 μm. The second version is the self-scanned registration by a photo-diode array, which gives discretized information. We have found experiments of this kind in [25, 29, 30] and they are one-dimensional. although such diode array can in principle also be two-dimensional. The most important problem here is to have a sufficiently fine pitch two-dimensional detector which is able to reproduce the form of small objects without any preliminary hypothesis about this form [30] (ratio between diode and object dimensions at least 1/10), and a correct experiment of this kind is still not reported in the literature.

The aim of the present communication is to apply well known numerical and experimental procedures to one and the same grating in order to compare them and to obtain combined information about its focusing properties from a rarely exploited point of view. We try to follow in some detail off-meridional imaging abilities, to verify experimentally how images from elementary point sources are forming the image of the entrance slit as a whole, extending in this way the image analysis proposed in [20]. Besides this, we also prove the usefulness of two recently proposed simple formulae for focal blur dimension estimation.

Because the spot dimensions discussed here are much greater than the wavelength we limit our consideration only to geometrical optics.

2. Grating description

The grating under consideration is designed for a flat field spectrograph covering a wide spectral range—from 350 to 900 nm. The grating is holographically recorded in photoresist, developed and aluminized. The groove height and the local efficiency are maximum in the central region and decrease towards the periphery in a Gaussian-like manner [31]. The period in the centre is $d_0 = 1{\cdot}26135$ μm and the grating operates in the first order. The substrate is a part of a sphere, which has a radius of curvature $R = 210{\cdot}8$ mm. The diffractive area is circular with diameter $\Phi = 92$ mm. Locations of the source, grating and focal lines are shown schematically in figure 1.

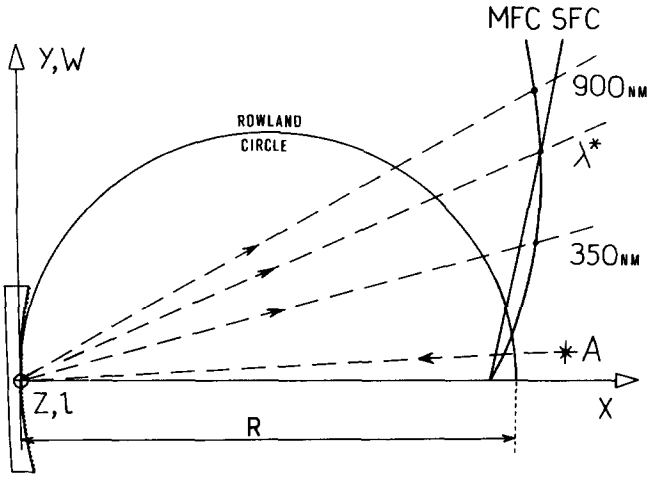

Figure 1. Schematic location of concave grating, focal curves (meridional MFC and sagittal SFC), Rowland circle, source A and coordinates systems $Oxyz$ and $Oxwl$.

The meridional and the sagittal focal curves (MFC, SFC) intersect each other only once in the operating interval—at $\lambda = \lambda^* = 570\,\text{nm}$. The two astigmatic coefficients F_{200}, F_{020} (this notation is explained below in the text) vanish there and the form and the dimensions of the focal spot are determined by the comatic aberration (figure 2). In all the remaining cases the image form, width and height are strongly dominated by the sagittal astigmatism so that classical and mixed coma are both masked. The possibility of examining different aberrations in a relatively pure form under equal conditions (varying only the wavelength) is an interesting advantage of concave gratings in contrast to classic lenses, where different specific experimental arrangements are necessary in order to create the different aberration images separately.

3. Experimental focal images

The fundamental information about the grating imaging properties is contained in the directly registered meridional focal spots resulting from a polychromatic point source.

We have chosen the photographic registration due to the following reasons:

(i) we need two-dimensional analogous information about the shape of the focal spots (the exact intensity distribution inside the spot is not of decisive importance for our purpose);

(ii) we need a technique with sufficient resolution—the photo plates have resolution of the order of 10 μm [21], while the diode array which we have in our disposal is one-dimensional and rather coarse—it has a period of 28 μm (16 μm sensitive length followed by 12 μm insensitive demarcation zone).

Care was taken to illuminate the grating as homogeneously as possible and to expose the photo plates properly in order to obtain focal spot images with clear contours. The dimensions of the images are measured by microscope with a relative accuracy of 10–15%, connected with the inevitable residual smoothness of the object boundaries.

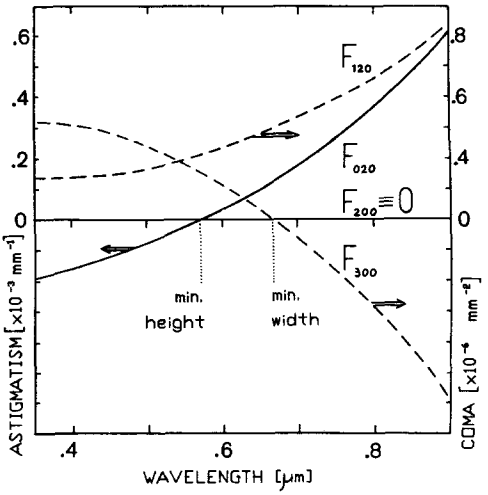

Figure 2. Spectral behaviour of the main aberration coefficients for the examined grating: meridional F_{200} and sagittal F_{020} astigmatism, classical F_{300} and mixed F_{120} coma.

We have used panchromatic ORWO Raman photo plates mounted on a micrometric holder, combined with a mechanical shutter. The function of a point source is performed by the 25× microscope objective with a 20 μm pinhole. Therefore the real source diameter is not zero as it would be in the ideal test situation, but varies for different wavelengths without exceeding 20 μm. Such a value is consistent with the pupil diameter or slit width values most often mentioned in the literature about concave gratings [4, 20, 21, 25, 27, 28] and it therefore permits comparisons with other data of this kind.

The illuminating beam is divergent and all the diffracted beams are at first convergent and then divergent when they propagate away from the grating; in the transition points they have their meridional (and sagittal) focus, there the photo plate is situated. The following set of laser lines is used: He–Cd (441·6 nm), Ar^+ (457·9 nm, ..., 514·5 nm), dye (570 nm), He–Ne (632·8 nm) and Kr^+ (647·1 nm, 676·4 nm).

Some typical spot photographs are presented in figure 3. The source is lying in the main (meridional, tangential, horizontal) plane—a case denoted further on as a 'meridional source'. An ideal image would be a circle of diameter nearly 20 μm. As was expected, however, practically all the images have a typically astigmatic deformation; only at $\lambda=\lambda^*$ the spot has obviously a comatic deformation. The measured width $W(\lambda)$ and height $H(\lambda)$ of the spots are plotted as experimental points depending on the wavelength in figures 5 and 6 respectively.

It is possible to model the grating behaviour under slit illumination by a set of point source images: the point source A is located successively at distances $z_a=0, 1, 2, 3$ mm out of the meridional plane ('off-meridional source') and its images are detected on one and the same photo plate. The result is shown on figure 4 for $\lambda=441{\cdot}6$, 570 and 632·8 nm. The geometric envelope of such a spot set gives an idea of the form of the upper half of the slit image; the lower half is symmetrical with respect to the meridional plane Oxy. It is clear that along the vertical direction the slit image is narrowest in its centre, where it intersects the plane Oxy; at its two ends the

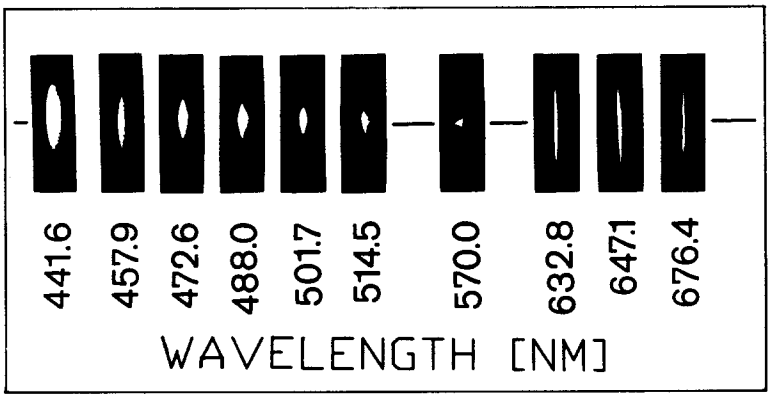

Figure 3. Photographs of meridional focal spots formed by a meridional point source at different wavelengths.

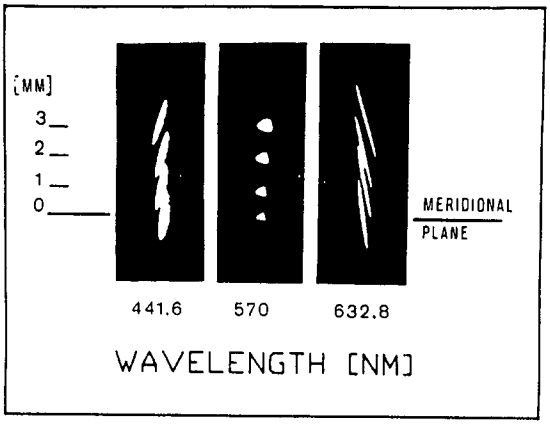

Figure 4. Photographs of focal spots created by a point source placed successively at $z_a = 0, 1, 2, 3$ mm out of the meridional plane Oxy.

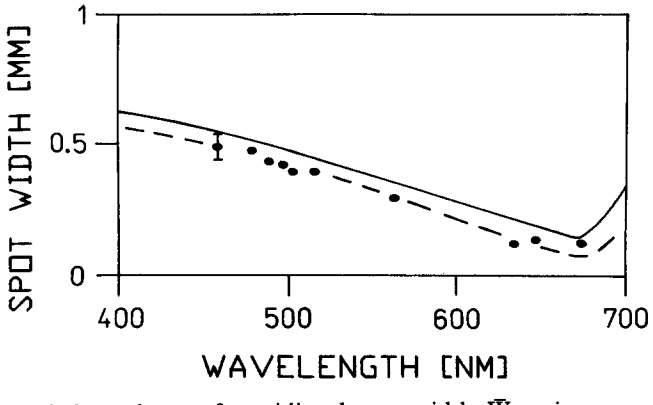

Figure 5. Spectral dependence of meridional spot width $\bar{W}$: points—measured values, dashed line—ray tracing prediction, continuous line—analytical estimations according to the formula (7 *a*).

spectral line becomes wider due to the enlargement and/or tilting of the individual off-meridional point source images.

The entire image height is connected with the slit height by the simple relations for the magnification of a spherical mirror [27, 28]:

$$H_a/H_b^M = r_a/r_b^M,$$

where H_a is the slit height, H_b^M is the focal image height, r_a and r_b are distances from the grating vertex to the entrance slit and to its focal image, respectively.

4. Ray tracing

Ray tracing is nowadays the most popular way to model optical systems—focusing gratings included—numerically [4, 6–19]. We assume a conical set of rays, emerging from an ideal point source and reaching the grating in certain points located on several (six in our case) concentric circles—so a divergent beam is simulated. Each ray undergoes reflection according to the mirror optics and to the conical diffraction optics. All the diffracted rays hit the image plane forming a point diagram and its envelope represents the focal spot contour.

Some diagrams for the grating under examination are shown in figure 7 (meridional point source) and figure 8 (off-meridional point source). The comparison between figures 3, 4 and 7, 8 convinces us about the good qualitative and quantitative correspondence between the experiment and the ray tracing predictions. The predicted spot dimensions are presented in figures 5, 6 by dashed lines.

Better agreement can be noted for the spot width—the real focal spots are more homogeneous and strongly outlined in meridional (horizontal) direction, which permits the width measurement to be more precise. The exposure which ensures more accurate height determination leads, unfortunately, to non-desirable overexposure of the overall image in meridional cross-section, i.e. to large errors in width determination.

The minimum spot width appears at $\lambda = 676$ nm—the measured value is close to 100 μm and the ray tracing prediction is close to 50 μm. One possible reason for such discrepancy is the non-zero diameter of the point source. Another possible reason is the eventual non-coincidence between the recording and/or operating parameters included in the ray tracing programme and their real values.

Summarizing we could say that ray tracing describes the observed focal spots in the general case (for meridional and off-meridional source location) well even if an ideal point source is assumed, but it is necessary to take into account the real source dimensions in the situations where the main aberrations (meridional F_{200} and sagittal F_{020} astigmatism) tend to zero simultaneously. One has also to determine carefully the exact real parameter values representing the input data for the ray tracing programme.

5. Analytical estimations

Analytical techniques are applied to many problems in concave grating performance. Most often the following themes are discussed: optimization of ruled area dimensions, resolution, focal curves, stigmatic conditions, slant angle of the spectral line, spectral behaviour of the aberration coefficients. Relatively rarely, however, the researchers attention has been directed to the influence of each aberration on the form and on the dimensions of the image of a meridional point

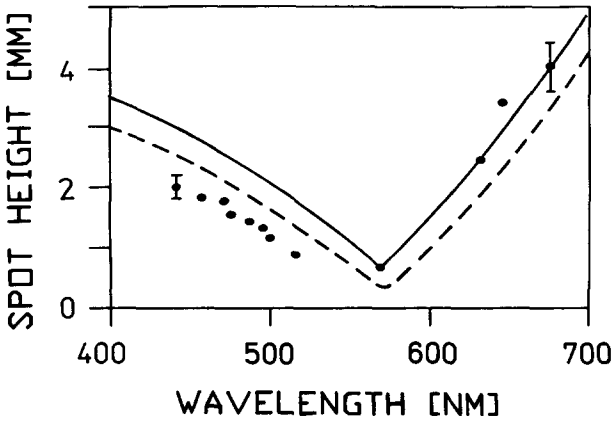

Figure 6. Same as figure 5, but for meridional spot height H and according to the formula (7 *b*).

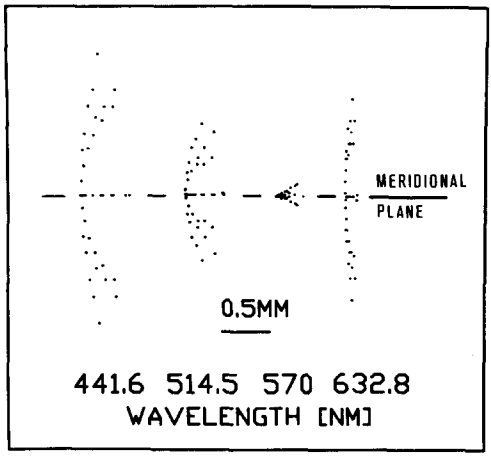

Figure 7. Ray tracing focal spot diagrams generated by a meridional ideal point source for some wavelengths.

source [32–34]. Some authors derive concrete expressions for the image height, but not about its width [16, 35]. Not one of the results referenced here have been checked by experiment or by ray tracing.

We have found only one article [36] treating explicitly analytically the form and the dimensions of the focal spot by a technique, well developed for lenses and presented in many textbooks, e.g. [37, 38]. In [36] the point source is supposed to be a meridional one and the image deformations caused by coma and spherical aberration are investigated. We apply the same technique (according to [38]) very briefly and only on a qualitative level in order to examine the image of an off-meridional point source, considering astigmatism, and both classical and mixed coma. Then we present two recently proposed simple formulae which are derived in [39] on this basis and serve for estimation of image width and height. The qualitative and quantitative results are compared here with experimental data and with ray tracing diagrams.

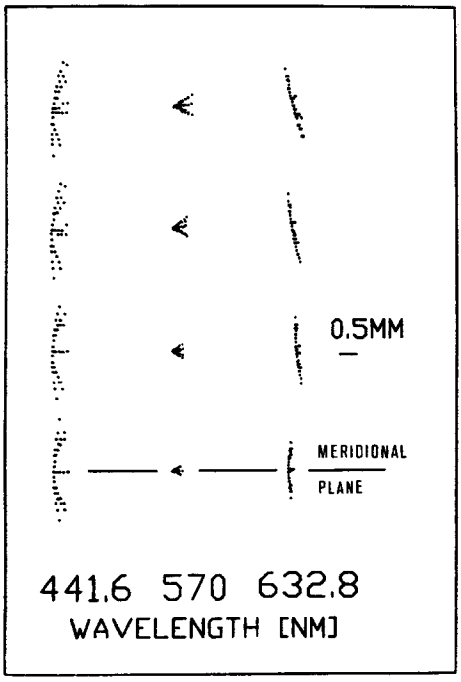

Figure 8. Ray tracing focal spot diagrams generated by an ideal point source placed successively at $z_a = 0, 1, 2, 3$ mm out of the meridional plane Oxy. Note that the 0·5 mm mark is valid only in respect to each individual spot; the distance between successive spots in vertical (sagittal—z or l) direction is intentionally enlarged for reasons of clarity.

The aberration function ΔF is expanded in a McLaurin series in powers of the meridional (w) and sagittal (l) grating (or pupil) coordinates [20]:

$$\Delta F(w, l, z_a) = \sum_{ij} w^i l^j \sum_k C_{ijk} F_{ijk}(z_a), \tag{1}$$

where z_a is the distance between the point source A and the meridional plane, C_{ijk} are normalization constants and F_{ijk} are the aberration coefficients given explicitly in [3, 20].

The image is described by the relative horizontal (h) and vertical (v) dimensionless aberration coordinates defined in the image plane, which are derived from ΔF approximately as its first partial derivatives [38, 40]:

$$h \approx \frac{\partial}{\partial w}(\Delta F); \qquad v \approx \frac{\partial}{\partial l}(\Delta F). \tag{2}$$

Combining (1) and (2) we obtain series expansions for h and v:

$$h = h^{(1)} + h^{(2)} + h^{(3)} + \ldots,$$

$$v = v^{(1)} + v^{(2)} + v^{(3)} + \ldots,$$

where $h^{(i)}$ (*or* $v^{(i)}$) includes all terms $w^p l^q$, where $p + q = i$.

If we consider only the first-order terms, we actually examine the combination of meridional and sagittal astigmatism (called also defocusing and astigmatism respectively):

$$h=h^{(1)}=w\,A(z_a)+l\,B(z_a),$$
$$v=v^{(1)}=w\,B(z_a)+l\,C(z_a), \tag{3}$$

where A, B, C are properly introduced simplifying notations:

$$A=(1/R)F_{200}+(1/2R^3)F_{202},$$
$$B=(1/R^2)F_{111}+(1/2R^4)F_{113},$$
$$C=(1/R)F_{020}+(1/2R^3)F_{022},$$

R is the radius of curvature of the grating blank [20].

When $z_a=0$ we have:

$$B=0, \qquad A=A_0=(1/R)F_{200}, \qquad C=C_0=(1/R)F_{020},$$

and therefore equations (3) are reduced to:

$$h=wA_0,$$
$$v=lC_0. \tag{4}$$

If we consider only the second-order terms, we examine the combination of classical and mixed coma:

$$h=h^{(2)}=w^2D(z_a)+wlE(z_a)+l^2F(z_a),$$
$$v=v^{(2)}=w^2(1/2)E(z_a)+wl2F(z_a)+l^2G(z_a), \tag{5}$$

where:

$$D=(1/2)[(3/R^2)F_{300}+(3/2R^4)F_{302}],$$
$$E=(1/R^3)F_{211}+(3/2R^5)F_{213},$$
$$F=(1/2)[(1/R^2)F_{120}+(3/2R^4)F_{122}],$$
$$G=(1/2)[(3/R^3)F_{031}+(3/2R^5)F_{033}].$$

When $z_a=0$ we have:

$$E=E_0=G=G_0=0,$$
$$D=D_0=(3/2R^2)F_{300}, \qquad F=F_0=(1/2R^2)F_{120},$$

and therefore equations (5) are reduced to:

$$h=w^2D_0+l^2F_0,$$
$$v=wl2F_0. \tag{6}$$

Usually concave gratings are designed so that the image is registered on the meridional focal curve or very close to it. Therefore the sagittal astigmatism dominates the image in the entire spectral interval excepting for one or two wavelengths λ^*, and in their vicinity, where the astigmatism tends to zero and only coma remains. We shall discuss these two typical situations separately, assuming that

w and l describe a system of concentric circles on the grating surface, as is shown in the left-hand side of figure 9.

Let us consider at first the astigmatic case. For a meridional point source ($z_a=0$) we use equation (4). Assuming $C_0 \gg A_0 > 0$ we obtain a typical vertically extended oval picture in the image plane, as is shown in figure 9 (a). When the source leaves the meridional plane ($z_a \neq 0$) equations (3) lead us to the picture in figure 9 (b) ($B=C \gg A>0$, $A>A_0$, $C>C_0$ is assumed). The main effect from the off-meridional source is immediately evident—its image is tilted with respect to the sagittal axis, exactly as is observed in our experiment (figure 4) and ray tracing diagrams (figure 8). So, together with the simple description of the optical effect we obtain an idea about the role of a group of aberration coefficients, namely F_{111}, F_{113}. The remaining F_{202}, F_{022} are simply variations of F_{200} and F_{020} and influence the length of the oval's axes.

Now we can discuss the comatic image—the experimental situation at the wavelength(s) λ^*. The image of a meridional point source described by equations (6) under the assumption $D_0 > F_0 > 0$ is shown in figure 9 (d)—it is a well known fan-shaped picture, symmetric in respect to the horizontal (meridional) plane. An off-meridional point source generates a pattern according to equation (5). ($E=G=D>F>0$, $D>D_0$, $F>F_0$ is assumed.) The image is fan-shaped again, but now it is rotated around its peak (figure 9 (c)). We have a good accordance with our experiment (figure 4, $\lambda=570$ nm) and ray tracing (figure 8, $\lambda=570$ nm). One can conclude that the coefficients F_{211}, F_{213}, F_{031}, F_{033} are connected with the rotation effect.

Nowadays such an analytical approach does not have a wide application in the process of grating design due to the existence of convenient direct numerical modelling techniques. For this reason we have described the off-meridional case only qualitatively, i.e. we have chosen the values of A, B, C, D, E, F, G as free parameters instead of calculating them using the corresponding explicit expressions. The analytical technique, however, maintains its own value, revealing the role of different aberration coefficients F_{ijk} and supporting the designer's intuition. No one of the two approaches replaces the other one, but they are most effective in combination.

Up to now we have discussed the form of the focal images. Concerning their dimensions, the ideology described above has been used already in [39] to derive a pair of estimation formulae. Therefore we shall simply apply them to our case, without explanations of derivation.

It is shown in [39] that the width $\bar{W}$ and the height $\bar{H}$ of the image B_0, generated on the meridional focal curve (MFC) by a meridional point source A are given approximately by the expressions:

$$\bar{W}=r_b^M\left(\frac{\Phi}{2}\right)^2\left(\frac{1}{2}\right)(3|F_{300}^M|+|F_{120}^M|), \tag{7a}$$

$$\bar{H}=2r_b^M\left[\left(\frac{\Phi}{2}\right)|F_{020}^M|+\left(\frac{\Phi}{2}\right)^2|F_{120}^M|\right]. \tag{7b}$$

Here r_b^M is the distance between grating vertex O and meridional focus B_0 determined from the equations $F_{100}=F_{200}=0$, F_{ij0}^M are the aberration coefficients calculated on the MFC and Φ is the diameter of the circular diffractive area. The quantity $\bar{W}$ presents eventually also the width of the spectral line.

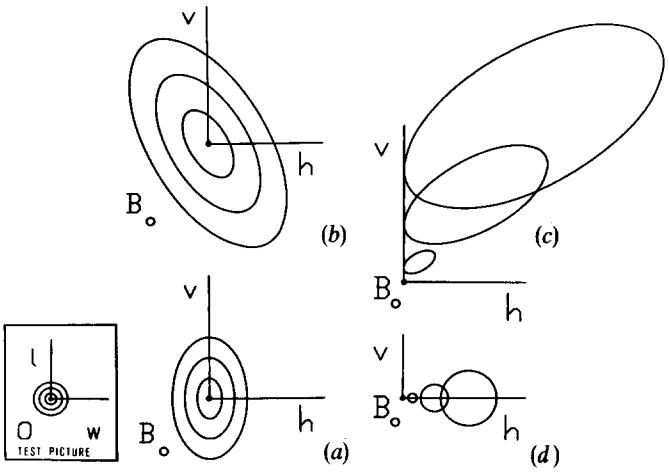

Figure 9. Schematic focal images generated from analytical considerations—formulae (3)–(6)—for qualitative understanding of image deformations due to different aberrations and to off-meridional point source location: [(*a*) and (*b*)]—pure astigmatism, [(*c*) and (*d*)]—pure coma, [(*a*) and (*d*)]—images of a meridional point source, [(*b*) and (*c*)]—images of an off-meridional point source. Test image in grating coordinates w, l is shown in the left-hand side.

The dimension values predicted by equations (7) are shown in figures 5, 6 with continuous lines together with experimental and ray tracing data. One can note the result is surprisingly good bearing in mind all the simplifications which are made deriving these expressions. Of course, we must not overrate this situation—it does not represent a proof for the universal validity of the formulae (7).

6. Conclusions

Focal images generated by a spherical holographic grating under point source illumination are photographically registered and measured for a set of wavelengths.

The results are compared with numerical (ray tracing) as well as with analytical (aberration function and coefficients) models of grating performance.

A satisfactory agreement between these approaches is observed. We could state that the numerical and the analytical approach complement each other for the understanding of each particular case. The ray tracing ensures more details and accuracy in the predictions, but one must be sure about the exact coincidence between input calculation parameters and real experimental parameters. The analytical method gives explicit connections between the most important quantities and stimulates the intuition, but it includes certain simplifications which can affect the results. Of course, the direct experimental observation of the focal images under real operating conditions retains its decisive role for the practical application of the grating.

The correspondence between experimental and ray tracing data and focal spot dimensions evaluated according to [39] is very good. This fact makes it possible for manufacturers as well as for users to estimate quickly and easily some important imaging characteristics.

References

[1] ROWLAND, H. A., 1882, *Phil. Mag.*, **13,** 469.
[2] ROWLAND, H. A., 1883, *Phil. Mag.*, **16,** 197.
[3] LOEWEN, E. G., 1983, *Applied Optics and Optical Engineering*, Volume IX, edited by R. R. Shannon and J. C. Wyant (New York: Academic Press), chap. II.
[4] LERNER, J. M., FLAMAND, J., LAUDE, J. P., PASSEREAU, G., and THEVENON, A., 1981, *Proc. SPIE*, **240,** 72.
[5] GOTO, K., KATO, Y., and TOGAWA, K., 1979, *Opt. Acta*, **26,** 841.
[6] STOZHAROVA, K. A., and ARISTOV, A. K., 1987, *Optiko-mekhanitcheskaya promyshlennost*, No. 4, 11 (in Russian).
[7] VILA, R., DE FRUTOS, A. M., and MAR, S., 1988, *Appl. Optics*, **27,** 3013.
[8] HARADA, T., and KITA, T., 1980, *Appl. Optics*, **19,** 387.
[9] MCKINNEY, W. R., and HOWELLS, M. R., 1980, *Nucl. Instrum. Meth.*, **172,** 149.
[10] IWANAGA, R., and OSHIO, T., 1979, *J. opt. Soc. Am.*, **69,** 1538.
[11] GOTO, K., KATO, Y., and TOGAWA, K., 1979, *Opt. Acta*, **26,** 841.
[12] TAKAHASHI, A., and KATAYAMA, T., 1978, *J. opt. Soc. Am.*, **68,** 1254.
[13] BITTNER, R., 1983, *Optik*, **64,** 185.
[14] BITTNER, R., 1986, *Proc. SPIE*, **655,** 206.
[15] GÜTHER, R., POLZE, S., and KORN, G., 1986, *Optik*, **72,** 71.
[16] BROWN, B. J., and WILSON, I. J., 1981, *Opt. Acta*, **28,** 1587.
[17] GÜTHER, R., 1984, *Opt. Applicata*, **14,** 429.
[18] WYNNE, C. G., 1982, *Opt. Acta*, **29,** 1557.
[19] SINGH, M., and REDDY, G. P., 1987, *Optik*, **76,** 83.
[20] NAMIOKA, T., SEYA, M., and NODA, H., 1976, *Japan J. appl. Phys.*, **15,** 1181.
[21] MEIJER, F. G., 1979, *J. Phys. E.*, **12,** 129.
[22] SEYA, M., 1952, *Science of Light* (Tokyo), **2,** 8.
[23] HARADA, T., MORIYAMA, S., and KITA, T., 1975, *Japan. J. appl. Phys.*, **14,** Suppl. 14–1, 175.
[24] HISA, M., and OSHIO, T., 1982, *Opt. Acta*, **29,** 1303.
[25] KITA, T., 1983, *J. Spectr. Soc. Japan*, **32,** 173 (in Japanese).
[26] SPEER, R. J., TURNER, D., JOHNSON, R. L., RUDOLPH, D., and SCHMAHL, G., 1974, *Appl. Optics*, **13,** 1258.
[27] KOIKE, M., and OHKUBO, K., 1986, *Appl. Optics*, **25,** 4071.
[28] POUEY, M., 1974, *J. Spectr. Soc. Japan*, **23,** Suppl. 1, 67.
[29] RIEGLER, G. R., and MORE, K. A., 1973, *IEEE Trans. nucl. Sci.*, **NS-20,** 102.
[30] FONCK, R. J., RAMSEY, A. T., and YELLE, R. V., 1982, *Appl. Optics*, **21,** 2115.
[31] LOEWEN, E. G., POPOV, E. K., TSONEV, L. V., and HOOSE, J., 1990, *J. opt. Soc. Am.* A, **7,** 1764.
[32] WERNER, W., 1967, *Appl. Optics*, **6,** 1691.
[33] ISHIGURO, E., IWANAGA, R., and OSHIO, T., 1979, *J. opt. Soc. Am.*, **69,** 1530.
[34] SINGH, M., and REDDY, G. P., 1987, *Optik*, **76,** 83.
[35] SINGH, M., and MAJUMDAR, K., 1970, *Optik*, **31,** 241.
[36] SHCHEPETKIN, YU. P., 1958, *Optika i Spektroskopiya*, **4,** 383 (in Russian).
[37] MARÉCHAL, A., 1956, *Handbook of Physics*, Volume XXIV, edited by S. Flügge (Berlin: Springer Verlag), chap. II.
[38] SLYUSAREV, G., 1968, *Methods for Optical System Calculation*, 2nd edition (Leningrad: Mashinostroenie) (in Russian).
[39] TSONEV, L., and POPOV, E., 1992, *Optics Commun.* (to be published).
[40] POUEY, M., 1983, *J. Optica, Paris*, **14,** 235.